Automatic Segmentation of Spinal Cord MS Lesions Across Multiple Sites, Contrasts and Vendors

Pierre-Louis Benveniste[1,2], Jan Valošek[1,2], Michelle Chen[1], Nathan Molinier[1,2], Lisa Eunyoung Lee[3,4], Alexandre Prat[5,6], Zachary Vavasour[7], Roger Tam[7], Anthony Traboulsee[8], Shannon Kolind[8], Jiwon Oh[3,4], Julien Cohen-Adad[1,2,9,10]

1. NeuroPoly Lab, Institute of Biomedical Engineering, Polytechnique Montreal, Montreal, QC, Canada
2. Mila - Quebec AI Institute, Montreal, QC, Canada
3. Department of Medicine (Neurology), University of Toronto, Toronto, ON, Canada
4. BARLO Multiple Sclerosis Centre & Keenan Research Centre, St. Michael's Hospital, Toronto, ON, Canada
5. Department of neuroscience, Université de Montréal, Montreal, QC, Canada
6. Neuroimmunology research laboratory, University of Montreal Hospital Research Centre (CRCHUM), Montreal, QC, Canada
7. School of Biomedical Engineering, University of British Columbia, Vancouver, BC, Canada
8. Departments of Medicine (Neurology), Physics, Radiology, University of British Columbia, Vancouver, BC, Canada
9. Functional Neuroimaging Unit, CRIUGM, Université de Montréal, Montreal, QC, Canada
10. Centre de Recherche du CHU Sainte-Justine, Université de Montréal, Montreal, QC, Canada

Introduction

Context:

- Clinical monitoring of spinal cord multiple sclerosis (MS) lesions is relevant for the early diagnostics and evaluation of MS progression [1].
- Few methods have tackled lesion segmentation in the spinal cord [2].
- Existing spinal cord MS lesion segmentation algorithms only work well for specific MRI contrasts but do not generalize well to other, previously unseen, contrasts.

Objectives:

- Develop a deep learning model for the automatic segmentation of spinal cord and MS lesions in PSIR and STIR contrasts images for longitudinal, multi-site and multi-vendor MRI data.
- Demonstrate the utility of the model to map spatio-temporal distribution of MS lesions across MS phenotypes.

Material & Methods

- **3T MRI** data from **5 sites** (Calgary, Edmonton, Montréal, Toronto and Vancouver) collected from ongoing ***Canadian Prospective Cohort Study to Understand Progression in MS (CanProCo)*** [3]
- **Sagittal phase sensitive inversion recovery (PSIR)** (4 sites, 333 participants) and **short tau inversion recovery (STIR)** (1 site, 92 participants) images of cervical spinal cord, both at 0.7×0.7×3 mm^3, from the baseline session (M0)
- Participants with both M0 and 12-month follow-up (M12) sessions: 158 relapsing-remitting MS (RRMS), 45 primary progressive MS (PPMS), and 45 radiologically isolated syndrome (RIS).

Image analysis:

- MS lesions and intervertebral discs were manually segmented on M0 images
- Spinal cord was automatically segmented on M0 images [4]
- Two **nnUNet** [5] models (2D and 3D) were trained on STIR and inverted PSIR (multiplied by -1) images from M0 to segment hyper-intense lesions and the spinal cord : 269/67/89 images for training/validation/testing.
- The models were evaluated against `sct_deepseg_lesion` [2] and then applied to unseen M12 data.
- For spatio-temporal lesion distribution: we brought lesion and spinal cord masks to the **PAM50 spinal cord template** [6] to create lesion probability maps for individual phenotypes and across sessions [7].

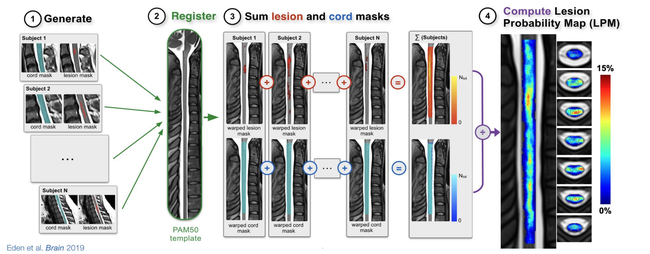

Figure 1: Mapping MS lesions in the spinal cord. Generated lesion and spinal cord masks are brought to the PAM50 spinal cord template. Registered masks are then summed. Finally, the Lesion Probability Map (LPM) is computed by averaging the sum of registered masks.

Results

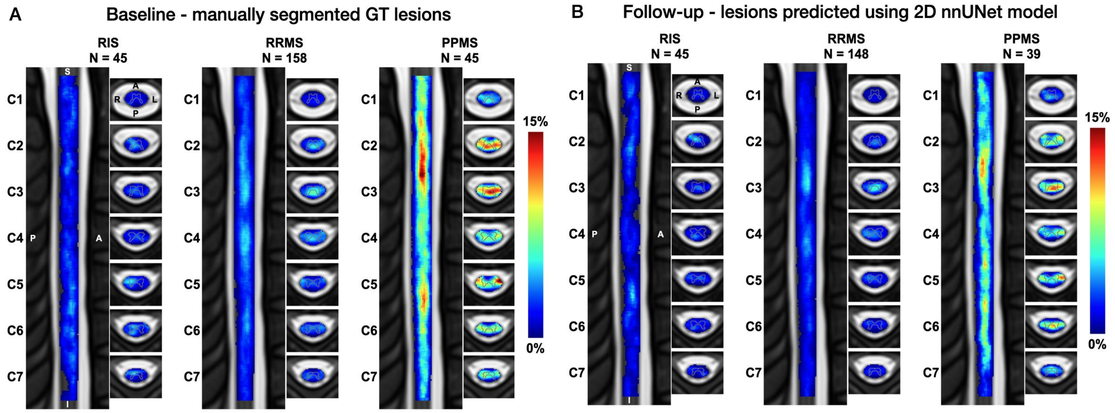

Figure 2: Probability maps of lesions in the cervical spinal cord across phenotypes. (A) Baseline (M0) map constructed from manually segmented lesions. (B) Map at follow-up (M12) built from the automatic lesion and spinal cord segmentation. The axial view shows an average of the lesion frequency across each vertebral level. The sagittal views show an average of the lesion frequency across sagittal slices. The gray matter contour is overlaid on the axial view. RIS = radiologically isolated syndrome, RRMS = relapsing-remitting MS, PPMS = primary progressive MS.

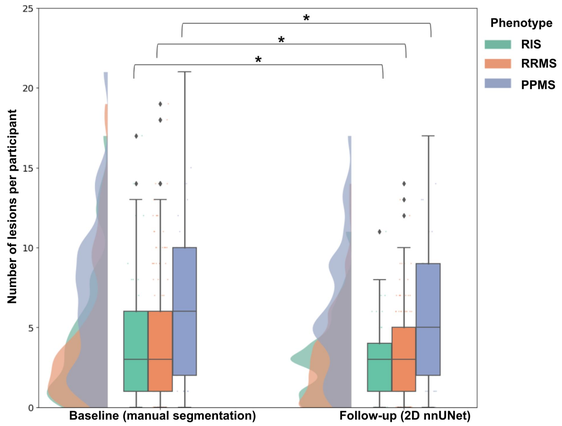

Figure 3: Distribution of lesion count per phenotype and time point. Lesion count is obtained from manual segmentation (for M0) and from the 2D nnUNet model (for M12). PPMS participants show a higher number of lesions relative to RRMS and RIS participants across all sessions. RIS = radiologically isolated syndrome, RRMS = relapsing-remitting MS, PPMS = primary progressive MS. *p-value < 0.05 (Wilcoxon signed-rank test).

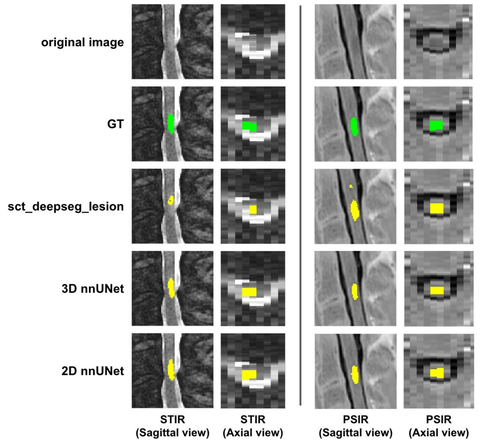

Figure 4: Qualitative examples of lesion segmentation in two representative subjects. The lesion segmentations results from `sct_deepseg_lesion`, the 3D nnUNet and the 2D nnUNet overlaid on the sagittal and axial views for STIR and PSIR contrasts. The left panel shows a lesion at level C3-C4; the right panel shows a lesion at level C2-C3.

Discussion & Conclusion

- Median Dice scores : 0.55 and 0.53 for the 2D and 3D models → similar to SOTA performance for SC MS lesion segmentation [2].
- The developed models outperformed `sct_deepseg_lesion` [2], keeping in mind that `sct_deepseg_lesion` was trained on different contrasts.
- Contrary to a previous longitudinal study showing an increase in lesion count in RRMS [8], our model predicted fewer lesions for M12 relative to M0. This is likely caused by a relatively low sensitivity of the model to detect lesions (median sensitivity is 0.5). This can be explained by: (i) the poorly defined lesions due to the highly anisotropic resolution, (ii) the aggregation of two different MRI contrasts for training a single model, and (iii) intra-rater variability in the generation of ground truth lesion masks [9].
- Similarly to previous studies [7,10], we found that lesions were more frequently located at C2-C3 and C5 vertebral levels, with a higher distribution of lesions in PPMS relative to RRMS and RIS. Further validation of the proposed models is needed to validate their performance against M12 manual segmentations.

Conclusion

- An automatic method for MS lesion segmentation from PSIR/STIR images.
- PPMS participants showed a higher number of lesions relative to RRMS and RIS participants across all sessions.
- In both the M0 (created from ground truth segmentations) and the M12 (created from predicted segmentations) maps, lesions were predominantly located at C2-C3 and C5 vertebral levels.

Future work:

- Manual segmentation of M12 results to improve our model performance
- Aggregation of more data for increased model generalizability
- Soft-segmentation to encode partial volume and output uncertainty information [11]

Acknowledgements

This research was supported by the Multiple Sclerosis Canada, Biogen Idec, Brain Canada, and Roche. We acknowledge all study participants as well as CanProCo collaborators. Thanks to Nick Guenther and Mathieu Guay-Paquet for helping with dataset management. We acknowledge Monica Stolar for designing the CanProCo logos. Funded by the Canada Research Chair in Quantitative Magnetic Resonance Imaging [CRC-2020-00179], the Canadian Institute of Health Research [PJT-190258], the Canada Foundation for Innovation [32454, 34824], the Fonds de Recherche du Québec - Santé [322736, 324636], the Natural Sciences and Engineering Research Council of Canada [RGPIN-2019-07244], the Canada First Research Excellence Fund (IVADO and TransMedTech), the Courtois NeuroMod project, the Quebec BioImaging Network [5886, 35450], INSPIRED (Spinal Research, UK; Wings for Life, Austria; Craig H. Neilsen Foundation, USA), Mila - Tech Transfer Funding Program. Contact: **pierre-louis.benveniste@polymtl.ca**

References

[1] Cortese et al., Mult. Scler. 24, 1536–1537 (2018). [2] Gros et al., Neuroimage 184, 901–915 (2019). [3] Oh et al., BMC Neurol. 21, 1–19 (2021). [4] Bédard et al., arXiv:2310.15402 [eess.IV] (2023). [5] Isensee et al., Nat. Methods 18, 203–211 (2021). [6] De Leener et al., Neuroimage 165, 170–179 (2018). [7] Eden et al., Brain 142, 633–646 (2019). [8] Zecca et al., Mult. Scler. 22, 782–791 (2016). [9] Walsh et al., 2023 IEEE 36th International Symposium on Computer-Based Medical Systems (CBMS) 463–470 (2023). [10] Kerbrat et al., Brain 143, 2089–2105 (2020). [11] Gros et al., Med. Image Anal. 71, 102038 (2021).